Weierstraß-Institut
für Angewandte Analysis und Stochastik
Leibniz-Institut im Forschungsverbund Berlin e. V.

Numerical methods for accurate description of ultrashort pulses in optical fibers

Shalva Amiranashvili[1], Mindaugas Radziunas[1], Uwe Bandelow[1],

Raimondas Čiegis[2]

submitted: January 16, 2018

[1] Weierstrass Institute Mohrenstr. 39 10117 Berlin Germany E-Mail: shalva.amiranashvili@wias-berlin.de. mindaugas.radziunas@wias-berlin.de uwe.bandelow@wias-berlin.de	[2] Vilnius Gediminas Technical University Saulėtekio al. 11 LT-10223 Vilnius Lithuania E-Mail: rc@vgtu.lt

Numerical methods for accurate description of ultrashort pulses in optical fibers

Shalva Amiranashvili, Mindaugas Radziunas, Uwe Bandelow,
Raimondas Čiegis

Abstract

We consider a one-dimensional first-order nonlinear wave equation (the so-called *forward Maxwell equation*, FME) that applies to a few-cycle optical pulse propagating along a preferred direction in a nonlinear medium, e.g., ultrashort pulses in nonlinear fibers. The model is a good approximation to the standard second-order wave equation under assumption of weak nonlinearity. We compare FME to the commonly accepted generalized nonlinear Schrödinger equation, which quantifies the envelope of a quickly oscillating wave field based on the slowly varying envelope approximation. In our numerical example, we demonstrate that FME, in contrast to the envelope model, reveals new spectral lines when applied to few-cycle pulses. We analyze and compare pseudo-spectral numerical schemes employing symmetric splitting for both models. Finally, we adopt these schemes to a parallel computation and discuss scalability of the parallelization.

1 Introduction

Propagation of *short* optical pulses in nonlinear fibers is adequately described by the generalized nonlinear Schrödinger equation (GNLSE), which applies to the pulse envelope [2, 14]. GNLSE is derived under the slowly varying envelope approximation (SVEA), such that pulse spectrum should be narrow, as compared to the value of the pulse carrier frequency. For an *ultrashort* (few-cycle) pulse or a sequence of short pulses at different frequencies the envelope concept becomes questionable [42], and, moreover, such an envelope is by no means slow. To follow the evolution of a spectrally broad wave packet one may equip GNLSE with additional terms (see, e.g., [16]). On the other hand, in some cases, the description provided by GNLSE becomes even worse after inclusion of additional terms [33]. An alternative approach is to avoid the use of a pulse envelope and to calculate the optical field directly. Several so-called *short pulse equations*, which are propagation models on the level of the electrical field, have been suggested [24, 31, 38, 8, 5, 27]. These models require special dispersion laws and in return have a rich analytic structure, e.g., they are either integrable [37, 34] or at least allow for an analytic description of solitary solutions [27, 39, 4]. Another class of useful field-level models has been derived for arbitrary dispersion relations [19, 23, 22, 21, 6]. Such equations provide the most accurate pulse description, but they have to be solved numerically.

Numerical algorithms for the solution of the GNLSE-type problems with most general nonlocal dispersion operator attracted recently a lot of attention. Comprehensive reviews on numerical methods for the GNLSE are available [9, 10], state of the art results for the related numerical splitting-type schemes are given in [30, 32, 40]. On the other hand, little is known about numerical approaches to the field-level short pulse equations, which are in the focus of this study.

In what follows we discuss a non-envelope unidirectional forward Maxwell equation (FME, see [19]) model. The latter is suitable for simulation of *ultrashort* optical pulses and spectrally broad wave pack-

ets in nonlinear fibers. The model employs unidirectional approximation to a general nonlinear wave equation; it is a valuable alternative to the common GNLSE, which is less general. Here we present an exemplary situation where the solution of the GNLSE for the pulse envelope considerably differs from the solution of the FME, what reveals limitations of the standard GNLSE model and demonstrates the potential of the FME approach.

The numerical schemes considered in our work are based on results of Ref. [7], where the efficiency of various numerical solvers of the GNLSE was studied. In the present work, we construct and apply pseudo-spectral symmetric splitting schemes with specialized approximations of different physical processes for both, GNLSE and FME models. We also propose an MPI-based parallelization of these algorithms and analyze the scalability of this parallelization. It is identified that the FFT parallel solver defines the efficiency of the parallel algorithm in the case of a distributed memory version of the solver.

The paper is organized as follows. In Section 2 we discuss a state of art non-envelope model for simulation of *ultrashort* optical pulses in nonlinear fibers. Numerical schemes based on pseudo-spectral and splitting methods for GNLSE and FME are constructed in Section 3. Example simulations of these two models and the comparison of the obtained results are performed in Section 4. Parallel versions of the numerical algorithms are proposed in Section 5. Conclusions are finally presented in Section 6.

2 Mathematical models

2.1 One-dimensional framework

For optical pulses in nonlinear media, the full pulse electric field $\mathbf{E}(\mathbf{r}, t)$ is often captured by a relatively simple $1+1$ dimensional scalar wave equation. In the first instance, this applies to a bulk propagation of a nonlinear plane wave with linear polarization. For instance, the wave may propagate along Oz axis such that the only non-vanishing electric and magnetic field components are $E_x = E(z, t)$ and $B_y = B(z, t)$. Assuming a typical cubic nonlinear polarization and a non-magnetic medium, pulse evolution is described by the one-dimensional reduction of the Maxwell equations [14]

$$\partial_z E = -\partial_t B, \qquad -\partial_z H = \partial_t D, \tag{1}$$

with the following material relations for the displacement field D and the magnetic field H,

$$D = \epsilon_0 \Big(\hat{\epsilon} E + \hat{\chi}^{(3)}[E, E, E] \Big), \qquad B = \mu_0 H.$$

Here ϵ_0 and μ_0 are vacuum permeabilities. Equations (1) are combined in a nonlinear wave equation

$$\partial_z^2 E - \frac{1}{c^2} \partial_t^2 \Big(\hat{\epsilon} E + \hat{\chi}^{(3)}[E, E, E] \Big) = 0, \tag{2}$$

where $c = (\epsilon_0 \mu_0)^{-1/2}$ is the speed of light. The operators $\hat{\epsilon}$ and $\hat{\chi}^{(3)}$ describe dispersion and non-linearity, respectively. Parameter z in the equations above denotes the spatial position at which the time-dependent fields are observed. In nonlinear optics it is convenient to take z as an evolutional coordinate [2, 14]. Thus, to close the problem (2) for $z \geq 0$, we supply the following initial conditions

$$E(z, t)|_{z=0} = E_0(t), \qquad \partial_z E(z, t)|_{z=0} = E_1(t). \tag{3}$$

The system (1) will be applied to a localized pulse, which vanishes for a fixed z and $t \to \pm\infty$. Both electric and magnetic field areas are then preserved in the sense that

$$\partial_z \int_{-\infty}^{\infty} E(z, t) dt = 0 \qquad \text{and} \qquad \partial_z \int_{-\infty}^{\infty} H(z, t) dt = 0.$$

A usual approximation (see discussion in [25]) is that both areas strictly vanish

$$\int_{-\infty}^{\infty} E(z,t)dt = 0 \qquad \text{and} \qquad \int_{-\infty}^{\infty} H(z,t)dt = 0, \tag{4}$$

which is assumed in our paper. In particular, we require that both

$$\int_{-\infty}^{\infty} E_0(t)dt = 0 \qquad \text{and} \qquad \int_{-\infty}^{\infty} E_1(t)dt = 0,$$

and, therefore,

$$\widetilde{E}(z,\omega)|_{\omega=0} = 0, \tag{5}$$

where the frequency-domain representation $\widetilde{E}(z,\omega)$ is related to the field function $E(z,t)$ through

$$\widetilde{E}(z,\omega) = \int_{-\infty}^{\infty} E(z,t)e^{i\omega t}dt, \qquad E(z,t) = \int_{-\infty}^{\infty} \widetilde{E}(z,\omega)e^{-i\omega t}\frac{d\omega}{2\pi}.$$

The dispersion operator $\hat{\epsilon}$ is a convolution operator. In the frequency domain it is quantified by the dispersion function $\epsilon(\omega)$. If the pulse field is decomposed into Fourier harmonics, the action of $\hat{\epsilon}$ is described by [26]

$$\hat{\epsilon}\, e^{-i\omega t} = \epsilon(\omega)e^{-i\omega t}, \qquad \hat{\epsilon}E(z,t) = \int_{-\infty}^{\infty} \epsilon(\omega)\widetilde{E}(z,\omega)e^{-i\omega t}\frac{d\omega}{2\pi}.$$

The latter expression is more tractable than convolution in the time domain, e.g., for spectrally narrow pulses.

A priori, $\epsilon(\omega)$ is a complex-valued function with the property $\epsilon(-\omega) = \epsilon^*(\omega)$, it's imaginary part represents dissipation. The latter is negligible in the so-called *transparency window*, a material-dependent interval of frequencies that are of special interest for optical applications, because of low absorption. In the transparency window, one can use Sellmeier's approximation [26]

$$\epsilon(\omega) = 1 + \sum_m \frac{B_m\lambda^2}{\lambda^2 - C_m}, \qquad \lambda = \frac{2\pi c}{\omega}, \tag{6}$$

with up to five terms in the sum for practically relevant cases [11]. Here, B_m and C_m are real-valued fit parameters. Both the transparency window and the pulse spectrum are well-separated from the singularities in Eq. (6). These singularities represent material resonances, at which dissipation becomes important.

The nonlinear operator $\hat{\chi}^{(3)}$ is associated with a kernel function $K(t_1,t_2,t_3)$ and is defined as

$$\hat{\chi}^{(3)}[E_1,E_2,E_3](z,t) = \iiint_{t_1,t_2,t_3=0}^{\infty} K(t_1,t_2,t_3)\times$$
$$E_1(z,t-t_1)E_2(z,t-t_2)E_3(z,t-t_3)\,dt_1dt_2dt_3.$$

$\hat{\chi}^{(3)}$ relates the nonlinear medium polarization to the prehistory of $E(z,t)$. We will be interested in two special situations. The simplest one corresponds to an instant cubic nonlinearity,

$$\hat{\chi}^{(3)}[E,E,E](z,t) = \chi E^3(z,t), \qquad \chi = \text{const.} \tag{7}$$

Here, the material constant χ is the nonlinear permeability of the third order. A more reliable situation corresponds to an instant response of electrons and a delayed Raman response of ions [2, 14]

$$\hat{\chi}^{(3)}[E, E, E](z, t) = \chi\Big((1 - f_R)E^2(z, t) + f_R \mathcal{I}(z, t)\Big)E(z, t),$$

$$\mathcal{I}(z, t) = \int_0^\infty R(t')E^2(z, t - t')dt'.$$

The weight factor f_R and the response function $R(t')$ are quantified in, e.g., Refs. [13, 43].

In addition to bulk propagation, Eq. (2) applies to optical fibers. For example, consider a single-mode fiber [2] in which the full electric field $\mathbf{E}(\mathbf{r}, t)$ can be factorized

$$\mathbf{E}(\mathbf{r}, t) \approx \mathbf{F}(x, y)E(z, t).$$

Here, the geometric factor $\mathbf{F}(x, y)$ is approximately the same for all frequencies in pulse spectrum. Two radial coordinates can be integrated out from Maxwell equations which are then reduced to Eq. (2) for the amplitude factor $E(z, t)$, see Ref. [12]. In this case, the effective $\epsilon(\omega)$ describes both the intrinsic medium dispersion and the geometric waveguide dispersion, and it results from a separate calculation that requires knowledge of the waveguide modes $\mathbf{F}(x, y)$, that depend parametrically on ω. In what follows. $\epsilon(\omega)$ is considered as a known function. It is taken real because power dissipation in silica fibers is as small as $0.2\,\text{dB/km}$ for a typical $\lambda = 1.55\,\mu\text{m}$ [41].

2.2 Unidirectional approximation

Although Eq. (2) looks simple, its numerical solution may be a challenge because (2) resolves fields on the wavelength scale ($\sim 1\,\mu\text{m}$), whereas the fiber length may reach hundreds of meters. We face a multi-scale problem and a simplified solution is highly desirable. Fortunately, Eq. (2) has an important feature: $\chi E^2 \ll 1$ for pulse powers that do not destroy the medium. A typical solution of Eq. (2) in this case is a combination of weakly nonlinear pulses, which propagate forward and backward along Oz axis almost unaware of each other. The mathematical formulation can be gained by using operators related to the refraction index $n(\omega)$ and the wave vector (propagation constant) $\beta(\omega)$, where

$$n(\omega) = \sqrt{\epsilon(\omega)}, \qquad \beta(\omega) = \frac{\omega}{c}n(\omega). \tag{8}$$

The operator $\hat{n}$ is derived from $n(\omega)$ in a full analogy with $\hat{\epsilon}$:

$$\hat{n}e^{-i\omega t} = n(\omega)e^{-i\omega t}, \qquad \hat{n}E(z, t) = \int_{-\infty}^\infty n(\omega)\widetilde{E}(z, \omega)e^{-i\omega t}\frac{d\omega}{2\pi},$$

evidently $\hat{\epsilon} = \hat{n}^2$. We also define the operator $\hat{\beta} = (1/c)\hat{n}\partial_t$ such that

$$\hat{\beta}e^{-i\omega t} = -i\beta(\omega)e^{-i\omega t}, \qquad \hat{\beta}E(z, t) = -i\int_{-\infty}^\infty \beta(\omega)\widetilde{E}(z, \omega)e^{-i\omega t}\frac{d\omega}{2\pi}. \tag{9}$$

The difference between $\hat{\epsilon}$ and $\hat{n}$ on one side and $\hat{\beta}$ on the other side is due to the fact that $\epsilon(-\omega) = \epsilon^*(\omega)$ and $n(-\omega) = n^*(\omega)$, whereas $\beta(-\omega) = -\beta^*(\omega)$ in accord with (8). Since $\widetilde{E}(z, -\omega) = \widetilde{E}^*(z, \omega)$ for a real-valued $E(z, t)$, one can easily find that $\hat{\beta}E(z, t)$ is real-valued as well. Note, that the zero-area condition (4) makes it possible to define

$$\hat{\beta}^{-1}E(z, t) = i\int_{-\infty}^\infty \frac{\widetilde{E}(z, \omega)}{\beta(\omega)}e^{-i\omega t}\frac{d\omega}{2\pi},$$

because the singularity at $\omega = 0$ is removable for a smooth $\widetilde{E}(z, \omega)$ due to Eq. (5).

Now we write Eq. (2) in the form

$$\left(\hat{\beta}^2 - \partial_z^2\right)E + \frac{1}{c^2}\partial_t^2\left(\hat{\chi}^{(3)}[E, E, E]\right) = 0. \tag{10}$$

The first (linear) term can be factorized and defines two special solutions of the linearized equation:

- forward propagating wave which is a linear combination of the functions $e^{i(kz-\omega t)}$, $k = \beta(\omega)$, and satisfies the equation $(\hat{\beta} + \partial_z)E = 0$, and

- backward propagating wave which is a combination of the functions $e^{i(kz-\omega t)}$, $k = -\beta(\omega)$, and satisfies the equation $(\hat{\beta} - \partial_z)E = 0$.

The second (nonlinear) term in Eq. (10) couples forward and backward waves and makes their strict definition more sophisticated. To this end, we start with a solution $E(z, t)$ of Eq. (10) and define its forward, $\underset{\rightarrow}{E}(z, t)$, and backward, $\underset{\leftarrow}{E}(z, t)$, components as solutions of the following *linear* equations

$$\left(\hat{\beta} + \partial_z\right)\underset{\rightarrow}{E} + \frac{1}{2c}\hat{n}^{-1}\partial_t\left(\hat{\chi}^{(3)}[E, E, E]\right) = 0, \tag{11}$$

$$\left(\hat{\beta} - \partial_z\right)\underset{\leftarrow}{E} + \frac{1}{2c}\hat{n}^{-1}\partial_t\left(\hat{\chi}^{(3)}[E, E, E]\right) = 0, \tag{12}$$

satisfying the initial conditions

$$\underset{\rightarrow}{E}(z, t)|_{z=0} = \frac{E_0(t) - \hat{\beta}^{-1}E_1(t)}{2} \quad \text{and} \quad \underset{\leftarrow}{E}(z, t)|_{z=0} = \frac{E_0(t) + \hat{\beta}^{-1}E_1(t)}{2}, \tag{13}$$

where we recall that the zero-area condition yields $\int_{-\infty}^{\infty} E_1(t)dt = 0$ and makes it possible to define $\hat{\beta}^{-1}E_1$. Furthermore, by applying $\hat{\beta} - \partial_z$ to Eq. (11) and $\hat{\beta} + \partial_z$ to Eq. (12), adding both resulting equations, recalling that $\hat{\beta} = (1/c)\hat{n}\partial_t$, and comparing the resulting equation to Eq. (10) we obtain

$$\left(\hat{\beta}^2 - \partial_z^2\right)\left[\underset{\rightarrow}{E}(z, t) + \underset{\leftarrow}{E}(z, t) - E(z, t)\right] = 0.$$

The initial conditions for the difference $\underset{\rightarrow}{E} + \underset{\leftarrow}{E} - E$ are trivial because Eqs. (3) and (13) yield

$$\underset{\rightarrow}{E}(z, t)|_{z=0} + \underset{\leftarrow}{E}(z, t)|_{z=0} = E_0(t) = E(z, t)|_{z=0},$$

and Eqs. (11) and (12) yield

$$\partial_z\underset{\rightarrow}{E}(z, t)|_{z=0} + \partial_z\underset{\leftarrow}{E}(z, t)|_{z=0} = \hat{\beta}\underset{\leftarrow}{E}(z, t)|_{z=0} - \hat{\beta}\underset{\rightarrow}{E}(z, t)|_{z=0} = E_1(t) = \partial_z E(z, t)|_{z=0}.$$

We conclude that the field $E(z, t)$ is a sum of the above defined forward and backward waves,

$$E(z, t) = \underset{\rightarrow}{E}(z, t) + \underset{\leftarrow}{E}(z, t). \tag{14}$$

Now we can substitute the expression (14) into Eqs. (11) and (12), which become a coupled system of *nonlinear* equations that can be solved without any *a priori* knowledge of the solution to Eq. (10).

The system (11), (12), in which $E(z, t)$ is eliminated using Eq. (14), is advantageous for considering of solely forward (backward) waves. Let ε be a small parameter related to the amplitude of the forward

wave and assume that an initial $\underset{\leftarrow}{E}(z,t)|_{z=0} = O(\varepsilon^3)$. Equation (12) suggests that also for $z > 0$ the amplitude of the nonlinearly generated backward wave scales as

$$\underset{\leftarrow}{E} \sim \hat{\chi}^{(3)}[\underset{\rightarrow}{E}, \underset{\rightarrow}{E}, \underset{\rightarrow}{E}] = O(\varepsilon^3).$$

The effect of the backward waves in Eq. (11) is then of the order of

$$\hat{\chi}^{(3)}[\underset{\rightarrow}{E}, \underset{\rightarrow}{E}, \underset{\leftarrow}{E}] = O(\varepsilon^5),$$

i.e., beyond the accuracy of the original Eq. (2) with only cubic nonlinearity. Therefore we neglect the backward wave in Eq. (11) and obtain a first-order unidirectional propagation equation for the forward wave

$$(\partial_z + \hat{\beta})\underset{\rightarrow}{E} + \frac{1}{2c}\hat{n}^{-1}\partial_t\Big(\hat{\chi}^{(3)}[\underset{\rightarrow}{E}, \underset{\rightarrow}{E}, \underset{\rightarrow}{E}]\Big) = 0. \tag{15}$$

From now on we don't distinguish between the forward wave field $\underset{\rightarrow}{E}(z,t)$ and the full field $E(z,t)$. Note that the just derived equation has the structure of the conservation law

$$\partial_z E + \partial_t\left(\frac{1}{c}\hat{n}E + \frac{1}{2c}\hat{n}^{-1}\hat{\chi}^{(3)}[E, E, E]\right) = 0,$$

such that the "forward area" $\int_{-\infty}^{\infty} E(z,t)dt$ is constant. For the instantaneous Kerr nonlinearity (7) we have

$$\partial_z E(z,t) + \hat{\beta}E(z,t) + \frac{\chi}{2c}\hat{n}^{-1}\partial_t\Big(E^3(z,t)\Big) = 0. \tag{16}$$

In the frequency domain the latter equation reads as

$$i\partial_z \widetilde{E}(z,\omega) + \beta(\omega)\widetilde{E}(z,\omega) + \frac{\chi\omega}{2cn(\omega)}\int_{-\infty}^{\infty} E^3(z,t)e^{i\omega t}dt = 0. \tag{17}$$

Equation (15) was originally derived in Ref. [19] by starting with Eq. (10) and setting (in our notations)

$$\hat{\beta}^2 - \partial_z^2 = 2\hat{\beta}(\hat{\beta} + \partial_z) - (\hat{\beta} + \partial_z)^2 \approx 2\hat{\beta}(\hat{\beta} + \partial_z),$$

because $(\hat{\beta} + \partial_z)E \to 0$ for a weakly nonlinear forward wave. In contrast to the derivation of Eq. (15) given in Ref [19] (see also Refs. [23, 22, 21, 6]), our derivation given above employs less mathematical assumptions, and in particular clearly distinguishes between forward and backward waves. In this way it offers an initial condition and an explicit estimate of the neglected terms.

Equations (15) and (16) can be further simplified by utilizing the fact that the index of refraction does not change much in the transparency window. For instance, for bulk fused silica the change in $n(\omega)$ is only 10% for more than 4 octaves in the frequency domain [11]. Consequently, dispersion of the nonlinear term in Eq. (15) can be ignored. The operator $\hat{n}^{-1}$ is then replaced by a factor n_*^{-1} for some characteristic value n_* of the refractive index. We will use the standard notation [2]

$$n_2 = \frac{3\chi}{8n_*}$$

for the nonlinear refractive index. In contrast to $\hat{n}^{-1}$, the time derivative of the nonlinear term in Eq. (15) cannot be simplified for short optical pulses, which are wide in the frequency domain. This time derivative describes self-steepening of pulses [2, 14].

A common way to deal with Eq. (15) is to solve it along the propagation coordinate z in a suitable time window that moves with the optical pulse. Therefore it is profitable to change from the time variable t to time delay τ by setting

$$E(z,t) = F(z,\tau) \quad \text{with} \quad \tau = t - z/V, \tag{18}$$

where V refers to a typical velocity that serves for a whole pulse or a sequence of pulses. Usually it is possible to introduce the carrier frequency ω_C and set

$$n_* = n(\omega_C), \qquad V = \frac{1}{\beta'(\omega_C)} = \left(\frac{d\omega}{dk}\right)_{\omega=\omega_C}. \tag{19}$$

Transformation (18) can be utilized in the frequency domain, where

$$F(z,\tau) \;\mapsto\; \widetilde{F}(z,\omega) = \int_{-\infty}^{\infty} F(z,\tau)e^{i\omega\tau}d\omega =$$

$$\int_{-\infty}^{\infty} E(z,t)e^{i\omega(t-z/V)}d\omega = \widetilde{E}(z,\omega)e^{-i\omega z/V}. \tag{20}$$

Therefore Eq. (17) yields

$$i\partial_z\widetilde{F}(z,\omega) + B(\omega)\widetilde{F}(z,\omega) + \frac{4n_2\omega}{3c}\int_{-\infty}^{\infty} F^3(z,\tau)e^{i\omega\tau}d\tau = 0,$$
$$B(\omega) = \beta(\omega) - \frac{\omega}{V}, \tag{21}$$

where $B(\omega)$ is just a Doppler-shifted propagation factor in the moving frame. Returning to the physical space in Eq. (21), we obtain that $F(z,\tau)$ is governed by the FME [19]

$$\partial_z F + \left(\hat{\beta} - V^{-1}\partial_\tau\right)F + \frac{4n_2}{3c}\partial_\tau\left(F^3\right) = 0. \tag{22}$$

The just derived FME is a natural competitor to the GNLSE

$$i\partial_z\psi + \hat{b}\psi + \frac{n_2}{c}(\omega_C + i\partial_\tau)|\psi|^2\psi = 0, \qquad \hat{b}\psi = \int_{-\infty}^{\infty} b(\Delta)\widetilde{\psi}(z,\Delta)e^{-i\Delta t}\frac{d\Delta}{2\pi},$$
$$b(\Delta) = \beta(\omega_C + \Delta) - \beta_0 - \beta_1\Delta, \qquad \beta_0 = \beta(\omega_C), \qquad \beta_1 = \beta'(\omega_C), \tag{23}$$

which in the simple case of Taylor approximation with respect to detuning Δ

$$b(\Delta) = \sum_{j=2}^{J}\frac{\beta_j}{j!}\Delta^j \quad\Leftrightarrow\quad \hat{b}\psi = \sum_{j=2}^{J}\frac{\beta_j}{j!}(i\partial_\tau)^j\psi,$$

is a standard pulse propagation equation in nonlinear fiber optics [2, 14]. Here, the carrier frequency ω_C is taken identical to that in Eq. (19) and

$$E(z,t) = \frac{1}{2}\psi(z,\tau)e^{i(\beta_0 z - \omega_C t)} + c.c., \quad \tau = t - \beta_1 z.$$

GNLSE models (23) can directly be derived from Eq. (2) by using the SVEA. It is noteworthy that GNLSE is solved in the frequency domain centered at ω_C, the most ambitious choice is $[0, 2\omega_C]$, see the upper part of Fig. 1. The frequency ω_M in this case is the maximal detuning from the carrier frequency. The GNLSE model (23) is opposed by the more general FME (22) which works in the frequency domain $[-\omega_M, \omega_M]$. The latter is typically several times larger than that of the GNLSE. We are especially interested in the differences between the FME and GNLSE and in physical situations that are correctly described only by the more general FME.
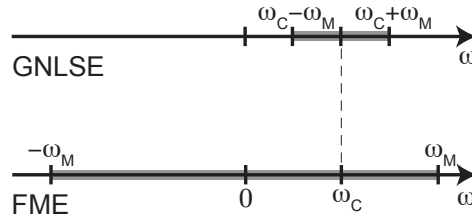
Figure 1: Schematic representation of frequencies resolved by the GNLSE and FME models.

3   Numerical schemes

First of all, we note that both the GNLSE problem (23) and the FME model (22) are defined within the infinite interval of the delay coordinate τ. When constructing numerical schemes, we restrict our study to the numerically tractable finite interval $[-\tau_R, \tau_R]$, where the length of the interval, $2\tau_R$, is inverse proportional to the resolution of the discrete frequencies. This time interval is covered by the discrete uniform grid

$$\bar{\Omega}_\tau = \left\{ \tau_j : \tau_j = jh, \quad j = -J/2, \ldots, J/2, \quad h = 2\tau_R/J \right\}$$

with the grid points denoted by τ_j, the grid boundary $\partial\Omega_\tau = \{\tau_{-J/2} = -\tau_R, \tau_{J/2} = \tau_R\}$, and the inner part of the grid $\Omega_\tau = \bar{\Omega}_\tau \backslash \partial\Omega_\tau$. When needed, we are also using the points $\tau_j = jh, |j| > J/2$, belonging to the extension of this grid over the boundaries of the domain. We will use a constant step h what allows us to apply the same grid for both finite difference and spectral methods. The choice of h should also be performed with care since it is inverse proportional to the maximal resolvable absolute (in the FME case) or relative (GNLSE case) field oscillation frequency ω_M, see Fig. 1.

Let Ω_z be a z-grid

$$\Omega_z = \left\{ z^n : z^n = z^{n-1} + \kappa_n, \quad n = 1, \ldots, N, \quad z^0 = 0, \quad z^N = L \right\},$$

where κ_n is the discretization step. For simplicity of notations in most definitions, we take the constant step-size $\kappa_n = \kappa$.

We consider numerical approximations U_j^n to the exact solution values $\psi_j^n = \psi(z^n, \tau_j)$ in the GNLSE case or $F_j^n = F(z^n, \tau_j)$ in the FME case at the grid points $(z^n, \tau_j) \in \Omega_z \times \bar{\Omega}_\tau$. To quantify nonlinear terms in these equations we introduce the symmetric finite difference operator

$$\partial_\tau^h U_j^n = \frac{U_{j+1}^n - U_{j-1}^n}{2h},$$

which, when needed, will be evaluated using the conditions

$$U_{-J/2}^n = U_{J/2}^n, \quad U_{-J/2-1}^n = U_{J/2-1}^n, \quad z^n \in \Omega_z. \tag{24}$$

With these periodic boundary conditions, we avoid artificial field reflections from the lateral boundaries at large z but feel an influence of the fields from the neighboring periods, instead.

Linear terms in both FME and GNLSE are treated in the frequency domain. Applying the spectral approximation numerical schemes, we use the following Fourier sum representation of the grid function U_j:

$$U_j = \left[\mathcal{F}^{-1}(\widehat{U}) \right]_j := \frac{1}{J} \sum_{\ell \in \mathbf{J}} \widehat{U}_\ell e^{-i\omega_\ell jh}, \quad j \in \mathbf{J} = \{-J/2, \ldots, J/2-1\}, \quad \omega_\ell = \frac{\pi\ell}{\tau_R},$$

where $\widehat{U}_\ell$ are the Fourier coefficients defined as

$$\widehat{U}_\ell = [\mathcal{F}(U)]_\ell := \sum_{j \in \mathbf{J}} U_j e^{i\omega_\ell jh}, \quad \ell \in \mathbf{J}. \tag{25}$$

3.1 Numerical schemes for GNLSE

Assuming that n is even, we approximate the GNLSE problem (23) using the following pseudo-spectral symmetric Strang splitting scheme [7, 18]:

$$
\begin{aligned}
&\widehat{U}_\ell^{n+\frac{1}{3}} = e^{i\kappa b(\omega_\ell)}\widehat{U}_\ell^n, \quad \ell \in \mathbf{J}, \\
&\frac{U_j^{n+\frac{2}{3}} - U_j^{n+\frac{1}{3}}}{\kappa} + \frac{n_2}{c}\partial_\tau^h \left(\left| \frac{U_j^{n+\frac{1}{3}} + U_j^{n+\frac{2}{3}}}{2} \right|^2 \frac{U_j^{n+\frac{1}{3}} + U_j^{n+\frac{2}{3}}}{2} \right) = 0, \quad j \in \mathbf{J}, \\
&U_j^{n+1} = \exp\left(i\kappa\frac{n_2}{c}\omega_C |U_j^{n+\frac{2}{3}}|^2 \right) U_j^{n+\frac{2}{3}}, \quad j \in \mathbf{J}, \\
&U_j^{n+\frac{4}{3}} = \exp\left(i\kappa\frac{n_2}{c}\omega_C |U_j^{n+1}|^2 \right) U_j^{n+1}, \quad j \in \mathbf{J}, \\
&\frac{U_j^{n+\frac{5}{3}} - U_j^{n+\frac{4}{3}}}{\kappa} + \frac{n_2}{c}\partial_\tau^h \left(\left| \frac{U_j^{n+\frac{4}{3}} + U_j^{n+\frac{5}{3}}}{2} \right|^2 \frac{U_j^{n+\frac{4}{3}} + U_j^{n+\frac{5}{3}}}{2} \right) = 0, \quad j \in \mathbf{J}, \\
&\widehat{U}_\ell^{n+2} = e^{i\kappa b(\omega_\ell)}\widehat{U}_\ell^{n+\frac{5}{3}}, \quad \ell \in \mathbf{J}.
\end{aligned}
\tag{26}
$$

In the second and fifth steps of this scheme, we exploit the periodic boundary conditions (24).

Next, we present main results on the approximation accuracy, stability and conservation laws valid for the discrete solution. The linear diffraction and local nonlinear interaction subproblems are solved exactly. Thus the discrete solutions of these subproblems satisfy the conservation laws:

$$\|U^{n+r/3}\|^2 = \|U^{n+(r-1)/3}\|^2, \quad r = 1, 3, 4, 6, \tag{27}$$

where the L_2 norm is defined as $\|U\|^2 = \sum_{j \in \mathbf{J}} |U_j|^2 h$.

The nonlinear advection subproblem is approximated using the second order accuracy implicit symmetric Euler scheme. It is solved using the following iterative procedure [28, 18]:

$$
\begin{aligned}
&\frac{\widetilde{U}_j^s - U_j^{n+\frac{1}{3}}}{\kappa} + \frac{n_2}{c}\partial_\tau^h \left(\left| \frac{\widetilde{U}_j^{s-1} + U_j^{n+\frac{1}{3}}}{2} \right|^2 \frac{\widetilde{U}_j^s + U_j^{n+\frac{1}{3}}}{2} \right) = 0, \quad j \in \mathbf{J}, \\
&\widetilde{U}_j^0 = U_j^{n+\frac{1}{3}}, \quad s = 1, \dots, S.
\end{aligned}
$$

For each iteration, a system of linear equations is solved, and the fast factorization algorithm is used. In all computer experiments, we have restricted to the predictor-corrector version of the algorithm when $S = 2$. It is important to note, that the symmetric Euler approximation scheme is unconditionally stable for the linear advection equation. This result follows trivially by using the Fourier analysis and Parseval's relation.

The considered nonlinear advection subproblems satisfy some conservation laws. It is well-known that transformations of the differential form into equivalent equations are valid only if the solution is

smooth. For weak solutions, such forms can be not equivalent. Thus we apply conservative methods to approximate the basic form of the equations. We note that the central difference approximation algorithm (26) can be presented in divergence form. We have approximated the nonlinear advection equation also by the explicit Richtmyer two-step Lax-Wendroff method [28]:

$$
U_{j+\frac{1}{2}}^{n+\frac{1}{2}} = \frac{1}{2}\left(U_j^{n+\frac{1}{3}} + U_{j+1}^{n+\frac{1}{3}}\right) - \frac{\kappa n_2}{2hc}\left(|U_{j+1}^{n+\frac{1}{3}}|^2 U_{j+1}^{n+\frac{1}{3}} - |U_j^{n+\frac{1}{3}}|^2 U_j^{n+\frac{1}{3}}\right),
$$

$$
U_j^{n+\frac{2}{3}} = U_j^{n+\frac{1}{3}} - \frac{\kappa n_2}{hc}\left(|U_{j+\frac{1}{2}}^{n+\frac{1}{2}}|^2 U_{j+\frac{1}{2}}^{n+\frac{1}{2}} - |U_{j-\frac{1}{2}}^{n+\frac{1}{2}}|^2 U_{j-\frac{1}{2}}^{n+\frac{1}{2}}\right), \quad j \in \mathbf{J}. \tag{28}
$$

The scheme (28) is also conservative, and it approximates the differential equation with the second order. Obviously, the explicit algorithm is only conditionally stable.

3.2 Numerical schemes for FME

In this case, we apply an only slightly modified approach, as for the GNLSE problem. Namely, we approximate the FME problem (22) using the following pseudo-spectral symmetric Strang splitting scheme

$$
\widehat{U}_\ell^{n+\frac{1}{2}} = e^{i\kappa B(\omega_\ell)}\widehat{U}_\ell^n, \quad \ell \in \mathbf{J},
$$

$$
\frac{U_j^{n+1} - U_j^{n+\frac{1}{2}}}{\kappa} + \frac{4n_2}{3c}\partial_\tau^h\left(\frac{U_j^{n+\frac{1}{2}} + U_j^{n+1}}{2}\right)^3 = 0, \quad j \in \mathbf{J},
$$

$$
\frac{U_j^{n+\frac{3}{2}} - U_j^{n+1}}{\kappa} + \frac{4n_2}{3c}\partial_\tau^h\left(\frac{U_j^{n+\frac{3}{2}} + U_j^{n+1}}{2}\right)^3 = 0, \quad j \in \mathbf{J}, \tag{29}
$$

$$
\widehat{U}_\ell^{n+2} = e^{i\kappa B(\omega_\ell)}\widehat{U}_\ell^{n+\frac{3}{2}}, \quad \ell \in \mathbf{J}.
$$

The nonlinear advection subproblems can be resolved using the iterative procedure,

$$
\frac{\widetilde{U}_j^s - U_j^{n+\frac{r}{2}}}{\kappa} + \frac{4n_2}{3c}\partial_\tau^h\left(\left[\frac{\widetilde{U}_j^{s-1} + U_j^{n+\frac{r}{2}}}{2}\right]^2 \frac{\widetilde{U}_j^s + U_j^{n+\frac{r}{2}}}{2}\right) = 0, \quad j \in \mathbf{J},
$$

$$
\widetilde{U}_j^0 = U_j^{n+\frac{r}{2}}, \quad s = 1,\dots,S, \quad r = 1,2,
$$

or can be approximated again by the explicit Richtmyer two-step Lax-Wendroff method:

$$
U_{j+\frac{1}{2}}^{n+\frac{r}{4}} = \frac{1}{2}\left(U_j^{n+\frac{r-1}{4}} + U_{j+1}^{n+\frac{r-1}{4}}\right) - \frac{4\kappa n_2}{6hc}\left([U_{j+1}^{n+\frac{r-1}{4}}]^3 - [U_j^{n+\frac{r-1}{4}}]^3\right),
$$

$$
U_j^{n+\frac{r+1}{4}} = U_j^{n+\frac{r-1}{4}} - \frac{4\kappa n_2}{3hc}\left([U_{j+\frac{1}{2}}^{n+\frac{r}{4}}]^3 - [U_{j-\frac{1}{2}}^{n+\frac{r}{4}}]^3\right), \quad j \in \mathbf{J}, \quad r = 3,5. \tag{30}
$$

The linear diffraction and linear advection interaction subproblems, both defined by the function $B(\omega)$ in the frequency domain, are solved exactly applying the spectral approach. Function $B(\omega)$ used in this case is defined in (21) and denotes a Doppler-shifted propagation factor in the moving frame. It is noteworthy, that the expression (25) for the zeroth Fourier component $\widehat{U}_\ell$ (with $\ell = 0$ and $\omega_\ell = 0$) is proportional to the discrete version of the field area within the computational domain,

$$
\widehat{U}_0^n = \sum_{j\in\mathbf{J}} U_j^n \approx \frac{1}{h}\int_{-\tau_R}^{\tau_R} F(z^n, \tau)\, d\tau.
$$

Thus, due to the condition $B(0) = 0$, the scheme (30) for the Fourier component $\widehat{U}_0$ provides the conservation of this discrete field area.

For the approximation of the basic form of nonlinear advection subproblem, we apply conservative methods. One can easily check that the summation of the central difference approximation algorithm (29), the corresponding iterative procedure, and the Lax-Wendroff method (30) over all $j \in \mathbf{J}$ provides the conservation condition for the discrete field area, $\sum_{j \in \mathbf{J}} U_j h$. This also proves the conservation of the discrete field area by the whole splitting scheme.

Finally, we note, that the approximation accuracy of the numerical scheme is of the second order with respect to both coordinates. In computational experiments, the accuracy was controlled using Runge rule and by repeating the computations with halved discretization steps.

4 Example

Example numerical solutions of the FME, which was solved using the splitting scheme combined with the two-step Lax-Wendroff method, and GNLSE models are compared in Fig. 2. We use $\beta(\omega)$ for bulk fused silica [11] and let the pulse circular frequency ω_C correspond to the wavelength $2.216\,\mu$m [$\nu_0 = \omega_C/(2\pi) = 135.3$ THz]. The initial pulse has a $\cosh^{-1}$ shape and is given by

$$E(z,\tau)|_{z=0} = \underbrace{\frac{\sqrt{P_0}}{\cosh(\tau/\tau_0)}}_{\psi(z,\tau)|_{z=0}} \sin(\omega_C \tau),$$

where $\tau_0 = 13$ fs. The seed pulse contains three oscillations of the wave field at half-maximum. The normalized initial peak power $n_2 P_0 = 0.0288$ is 60% larger than that of the fundamental soliton at frequency ω_C. Such a pulse cannot propagate without changes in its shape, as opposed by fundamental solitons [17].

The GNLSE solution, see Fig. 2(a,c), shows slowly decreasing power oscillations with the increase of z both in space-time [Fig. 2(a)] and space-frequency [Fig. 2(c)] domains. At maximum compression ($z = 1.5$ mm) of the pulse, its spectrum achieves its maximal width, which is sufficient for generation of a wave at the new frequency [650 THz in Fig. 2(c)], the so-called soliton's Cherenkov radiation [3]. The radiation is responsible for asymmetry of the pulse field in Fig. 2(a).

The FME solution is shown in Fig. 2(b,d). The space-time representation is similar to Fig. 2(a), whereas in the frequency domain we see notable differences. Not only the third harmonic of the carrier frequency becomes visible [at 400 THz in Fig. 2(d)] but also two new Cherenkov-type lines appear. Such lines attracted recently considerable attention [29, 15], their adequate explanation and accurate description are still under debate.

5 Parallel algorithm

In this section, we are considering and discussing the parallelization of all numerical solution algorithms presented in Section 3. Here we restrict to a strong scalability analysis when the size of the discrete problems is fixed and different numbers of processors are used in the computations. Such information is very important when a medium size problem should be solved as fast as possible. In
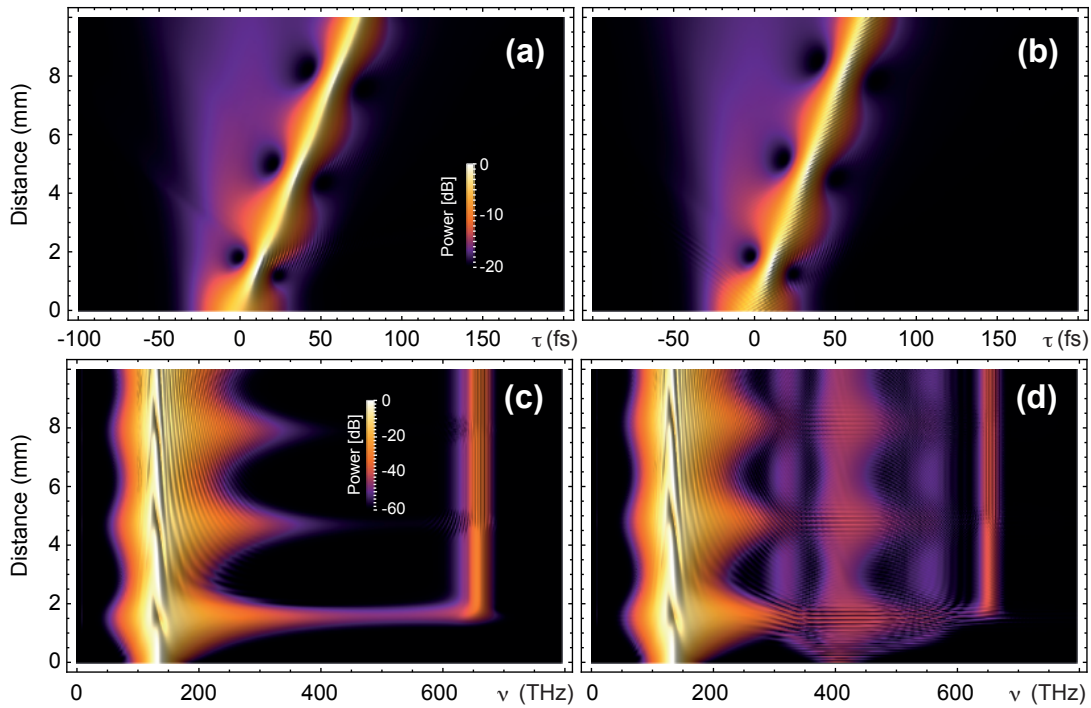
Figure 2: Exemplary solutions of the GNLSE (a,c) and FME (b,d) for a three-cycle pulse that propagates in fused silica. The energy density plots are given in space-time (a,b) and space-frequency (c,d) domains. See text for parameters and discussion.

order to estimate the general trend of a scalability analysis, we also present results for a problem with doubled size of the grid.

All parallel numerical tests in this work were performed on the computer cluster "HPC Sauletekis" (`http://www.supercomputing.ff.vu.lt`) at the High-Performance Computing Center of Vilnius University, Faculty of Physics. We have used nodes with Intel® Xeon® processors E5-2670 with 16 cores (2.60 GHz) and 128 GB of RAM per node. Computational nodes are interconnected via the InfiniBand network.

A standard method for the parallel solution of such problems is the domain decomposition method [35, 36]. We use a simple one-dimensional partitioning of the grid Ω_τ. The discrete mesh of the problem domain and associated sets of solutions are partitioned into sub-domains, which are allocated to different processes. The parallel algorithm is implemented using MPI library to cover both shared and distributed memory architectures of parallel computers [1].

Below we present a detailed description of the parallel algorithm for the pseudo-spectral symmetric Strang splitting scheme (26) used for the solution of the GNLSE problem. The advection problem is approximated by the explicit Richtmyer two-step Lax-Wendroff scheme (28). A parallel version of the splitting scheme (29) for the FME problem is constructed following the same template.

Let us assume that P processes are used. We decompose the computational grid $\bar{\Omega}_\tau$ and a set of indexes $\mathbf{J}$ into P non-overlapping size-balanced sub-grids Ω_τ^l and subsets $\mathbf{J}_l$, $l = 1, \ldots, P$:

$$\bar{\Omega}_\tau = \bigcup_{l=1}^{P} \Omega_\tau^l, \quad \mathbf{J} = \bigcup_{l=1}^{P} \mathbf{J}_l.$$

Then ℓ-th process should perform the following calculations ($\tilde{n}$ in the schemes below denotes the

starting index of each step):

1. Solve the local cubic nonlinearity subproblem:

$$U_j^{\tilde{n}+\frac{1}{3}} = \exp\left(i\kappa\frac{n_2}{c}\omega_C|U_j^{\tilde{n}}|^2\right)U_j^{\tilde{n}}, \quad j \in \mathbf{J}_\ell.$$

The algorithm is parallel and no data communication is required.

2. Solve the nonlinear advection subproblem: The

$$U_{j+\frac{1}{2}}^{\tilde{n}+\frac{1}{6}} = \frac{1}{2}\left(U_j^{\tilde{n}} + U_{j+1}^{\tilde{n}}\right) - \frac{\kappa n_2}{2hc}\left(\left|U_{j+1}^{\tilde{n}}\right|^2 U_{j+1}^{\tilde{n}} - \left|U_j^{\tilde{n}}\right|^2 U_j^{\tilde{n}}\right),$$

$$U_j^{\tilde{n}+\frac{1}{3}} = U_j^{\tilde{n}} - \frac{\kappa n_2}{hc}\left(\left|U_{j+\frac{1}{2}}^{\tilde{n}+\frac{1}{6}}\right|^2 U_{j+\frac{1}{2}}^{\tilde{n}+\frac{1}{6}} - \left|U_{j-\frac{1}{2}}^{\tilde{n}+\frac{1}{6}}\right|^2 U_{j-\frac{1}{2}}^{\tilde{n}+\frac{1}{6}}\right), \quad j \in \mathbf{J}_\ell.$$

The Richtmyer two-step Lax-Wendroff scheme is explicit, and all computations are done in parallel. The scheme is based on three-point grid stencil, thus the approximation of fluxes requires to exchange values of the solutions at boundaries of subdomains, including the periodicity conditions. The communication of overlapping data is done only among adjacent processes, and the well-known odd-even paradigm is used to implement it in parallel.

3. Solve the linear propagation subproblem:

$$\widehat{U}_s^{\tilde{n}} = e^{i\kappa b(\omega_s)}\widehat{U}_s^{\tilde{n}}, \quad s \in \mathbf{J}_\ell.$$

This algorithm is implemented in parallel and no communication is required.

The discrete FFT should be done before and after this step, and this transform is the most computation intensive part of the parallel algorithm. It takes about 56% of all CPU time. We have used the parallel version of FFTW library to implement the discrete FFT algorithm [20].

To test the parallel performance of the developed algorithm, we have solved GNLSE problem using two sizes of the discrete grid $J = 16384$, $N = 60000$ and $J = 32768$, $N = 120000$.

Parallel performance results of our parallel solver are presented in Table 1. The total wall time T_p is given in seconds, here p is the total number of used parallel processes. In Table 1, we also present the obtained values of parallel algorithmic speed-up $S_p = T_1/T_p$ and efficiency $E_p = S_p/p$.

Table 1: The total wall time T_p, speed-up S_p and efficiency E_p for solving GNLSE problem with two sizes of the discrete problem: small $J = 16384$, $N = 60000$ and large $J = 32768$, $N = 120000$.

$J = 16384, N = 60000$	$p = 1$	$p = 2$	$p = 4$	$p = 8$	$p = 16$
T_p	567	327	167	83	48
S_p	1	1.734	3.40	6.83	11.8
E_p	1	0.867	0.850	0.854	0.738
$J = 32768, N = 120000$	$p = 1$	$p = 2$	$p = 4$	$p = 8$	$p = 16$
T_p	2280	1300	632	331	188
S_p	1	1.75	3.61	6.89	12.1
E_p	1	0.877	0.902	0.861	0.758

The obtained speed-up and efficiency values of the parallel algorithm are satisfying; they show that the scalability of the algorithm is efficient, even for smaller size discrete problems. Some degradation of the efficiency is mainly connected to the challenges to parallelize the FFT algorithm. The parallel version of the FFTW algorithm shows a good scalability up to 16 processes when the shared memory version of MPI algorithm can be used. Even in this case, we see some degradation when $8 + 8$ cores (the case of $p = 16$ in Table 1) of two different processors in one node are used.

If this parallel algorithm is computed on two nodes with 32 processes, the distributed memory version of the FFTW algorithm is applied. The efficiency of the parallel algorithm, in this case, is seriously degraded, the larger problem is solved in $T_{32} = 283$ seconds, which is close to the time used for the same calculations by 8 processes. In order to show that the parallel efficiency of the remaining part of the algorithm is optimal, computational experiments are done for a larger problem with full nonlinearity but vanishing dispersion. The following results are obtained:

$$T_1 = 1002, \ \ T_2 = 504, \ \ T_4 = 253, \ \ T_8 = 129, \ \ T_{16} = 73, \ \ T_{32} = 37.$$

The algorithms are perfectly scalable even for distributed memory case when two nodes with 32 processes are used.

6 Conclusions

In this paper, we have presented a new derivation of the FME from the one-dimensional nonlinear wave equation, the latter is mathematically strictly decomposed in nonlinear forward and backward waves. Like in the case of GNLSE, the assumption of the single field propagation direction allows us to exploit time coordinate transformation (18) and to calculate the optical field evolution only in the finite comoving frame. This means that comparing to FME, the numerical solution of the full wave equation requires much more computational time and memory resources.

In contrast to GNLSE, however, the application of FME requires tracking the frequencies from a larger frequency range, as it was shown in Fig. 1, and, therefore, the calculation time needed to resolve FME usually is significantly larger than that one required by GNLSE. For ultrashort (a few optical cycle-long) pulses, for supercontinuum generation, or for the systems where several pulses with strongly differing carrier frequencies are present, all frequencies within the interval $[0, \omega_M]$ can be important. In this case, the time and memory resources required by GNSLE and FME become comparable. However, as we have shown in our example, in these situations, the conventional GNSLE can fail to show some effects, which, on the other hand, are still tracked by the FME.

The algorithms suggested for the numerical solution of both, GNLSE and FME models are based on the pseudo-spectral splitting scheme. Such scheme is a natural choice for numerical integration of both these models with nonlocal dispersion operators defined in the frequency domain. To speed up the calculations, we have tested our algorithms on a parallel computer cluster. We have found, that scalability of the parallel algorithm remains good until all exploited cores are on the same node and the shared memory version of the algorithm is used. This scalability was drastically degraded when the simulations were carried out on different nodes, and distributed memory version of the FFT algorithm was applied.

References

[1] Mpi forum, "mpi: A message passing interface standard". www.mpi-forum.org, 1995.

[2] G. P. Agrawal. *Nonlinear Fiber Optics*. Academic, New York, 4 edition, 2007.

[3] N. Akhmediev and M. Karlsson. Cherenkov radiation emitted by solitons in optical fibers. *Phys. Rev. A*, 51(3):2602–2607, 1995.

[4] Sh. Amiranashvili, U. Bandelow, and N. Akhmediev. Dispersion of nonlinear group velocity determines shortest envelope solitons. *Phys. Rev. A*, 84(4):043834, October 2011.

[5] Sh. Amiranashvili, U. Bandelow, and N. Akhmediev. Few-cycle optical solitary waves in nonlinear dispersive media. *Phys. Rev. A*, 87(1):013805, January 2013.

[6] Sh. Amiranashvili and A. Demircan. Ultrashort optical pulse propagation in terms of analytic signal. *Advances in Optical Technologies*, 2011:989515, November 2011.

[7] Sh. Amiranashvili, R. Čiegis, and M. Radziunas. Numerical methods for a class of generalized nonlinear Schrödinger equations. *Kinetic and Related Models*, 8(2):215–234, 2015.

[8] Sh. Amiranashvili, A. G. Vladimirov, and U. Bandelow. A model equation for ultrashort optical pulses around the zero dispersion frequency. *Eur. Phys. J. D*, 58(2):219–226, January 2010.

[9] X. Antoine, W. Bao, and Ch. Besse. Computational methods for the dynamics of nonlinear Schrödinger/Gross-Pitaevskii equations. *Comput. Phys. Commun.*, 184:2621–2633, 2013.

[10] W. Bao, Q. Tang, and Z. Xu. Numerical methods and comparison for computing dark and bright solitons in the nonlinear Schrödinger equation. *J. Comput. Phys.*, 235:423–445, 2013.

[11] M. Bass, E. W. Van Stryland, D. R. Williams, and W. L. Wolfe, editors. *Handbook of Optics*, volume 1. McGRAW-HILL, 2 edition, 1995.

[12] F. Biancalana, D. V. Skryabin, and P. St. J. Russell. Four-wave mixing instabilities in photonic-crystal and tapered fibers. *Phys. Rev. E*, 68(4):046603, October 2003.

[13] K. J. Blow and D. Wood. Theoretical description of transient stimulated Raman scattering in optical fibers. *IEEE J. Quantum Electron.*, 25(15):2665–2673, 1989.

[14] R. W. Boyd. *Nonlinear Optics*. Academic, New York, 3 edition, 2008.

[15] Matteo Conforti, Andrea Marini, Truong X. Tran, Daniele Faccio, and Fabio Biancalana. Interaction between optical fields and their conjugates in nonlinear media. *Opt. Express*, 21(25):31239–31252, 2013.

[16] J. M. Dudley, G. Genty, and S. Coen. Supercontinuum generation in photonic crystal fiber. *Rev. Mod. Phys.*, 78(4):1135–1184, 2006.

[17] Akira Hasegawa and Masayuki Matsumoto. *Optical Solitons in Fibers*. Springer, 2003.

[18] W. Hundsdorfer and J.G. Verwer. *Numerical Solution of Time-Dependent Advection-Difusion-Reaction Equations*, volume 33 of *Springer Series in Computational Mathematics*. Springer, Berlin, Heidelberg, New York, Tokyo, 2003.

[19] A. V. Husakou and J. Herrmann. Supercontinuum generation of higher-order solitons by fission in photonic crystal fibers. *Phys. Rev. Lett.*, 87(20):203901, 2001.

[20] S.G. Johnson and M. Frigo. A modified split-radix FFT with fewer arithmetic operations. *IEEE Trans. Signal Processing*, 55(1):111–119, 2007.

[21] P. Kinsler. Optical pulse propagation with minimal approximations. *Phys. Rev. A*, 81(1):013819, 2010.

[22] M. Kolesik and J. V. Moloney. Nonlinear optical pulse propagation simulation: From Maxwell's to unidirectional equations. *Phys. Rev. E*, 70(3):036604, 2004.

[23] M. Kolesik, J. V. Moloney, and M. Mlejnek. Unidirectional optical pulse propagation equation. *Phys. Rev. Lett.*, 89(28):283902, 2002.

[24] S. A. Kozlov and S. V. Sazonov. Nonlinear propagation of optical pulses of a few oscillations duration in dielectric media. *JETP*, 84(2):221–228, 1997.

[25] Victor V. Kozlov, Nikolay N. Rosanov, Costantino De Angelis, and Stefan Wabnitz. Generation of unipolar pulses from nonunipolar optical pulses in a nonlinear medium. *Phys. Rev. A*, 84(2):023818, 2011.

[26] L. D. Landau, E. M. Lifshitz, and L. P. Pitaevskii. *Electrodynamics of Continuous Media*. Elsevier, New York, 2 edition, 1984.

[27] H. Leblond and D. Michaelis. Models of few optical cycle solitons beyond the slowly varying envelope approximation. *Phys. Rep.*, 523(2):61–126, February 2013.

[28] R.J. LeVeque. *Numerical Methods for Conservation Laws.* Lectures in Mathematics. Birkhäuser, ETH Zürich, 1990.

[29] Cristian Redondo Loures, Andrea Armaroli, and Fabio Biancalana. Contribution of third-harmonic and negative-frequency polarization fields to self-phase modulation in nonlinear media. *Opt. Lett.*, 40(4):613–616, February 2015.

[30] C. Lubich. On splitting methods for schrödinger–poisson and cubic nonlinear schrödinger equations. *Math. Comput.*, 77:2141–2153, 2008.

[31] A. I. Maimistov. Some models of propagation of extremely short electromagnetic pulses in a nonlinear medium. *Quantum Electron.*, 30(4):287–304, 2000.

[32] Ch. Neuhauser and M.Thalhammer. On the convergence of splitting methods for linear evolutionary Schrödinger equations involving an unbounded potential. *BIT Numer. Math.*, 49:199–215, 2009.

[33] K. E. Oughstun and H. Xiao. Failure of the quasimonochromatic approximation for ultrashort pulse propagation in a dispersive, attenuative medium. *Phys. Rev. Lett.*, 78(4):642–645, 1997.

[34] M. Pietrzyk, I. Kanattŝikov, and U. Bandelow. On the propagation of vector ultra-short pulses. *J. Nonlinear Math. Phys.*, 15(2):162–170, 2008.

[35] A. Quarteroni and A. Valli. *A Domain Decomposition Methods for Partial Differential Equations*. Oxford Science Publications, 1999.

[36] M. Radziunas and R. Čiegis. Effective numerical algorithm for simulations of beam stabilization in broad area semiconductor lasers and amplifiers. *Math. Model. Anal.*, 19(5):627–646, 2014.

[37] A. Sakovich and S. Sakovich. The short pulse equation is integrable. *J. Phys. Soc. Jpn.*, 74(1):239–241, 2005.

[38] T. Schäfer and C. E. Wayne. Propagation of ultra-short optical pulses in cubic nonlinear media. *Physica D*, 196(1–2):90–105, 2004.

[39] S. A. Skobelev, D. V. Kartashov, and A. V. Kim. Few-optical-cycle solitons and pulse self-compression in a Kerr medium. *Phys. Rev. Lett.*, 99(20):203902, 2007.

[40] M. Thalhammer, M. Caliari, and Ch. Neuhauser. High-order time-splitting Hermite and Fourier spectral methods. *J. Comput. Phys.*, 228:822–832, 2009.

[41] K. Thyagarajan and A. Ghatak. *Fiber optic essentials*. John Wiley & Sons, 2007.

[42] D. E. Vakman and L. A. Vainshtein. Amplitude, phase, frequency — fundamental concepts of oscillation theory. *Usp. Fiz. Nauk*, 20(12):1002–1016, 1977.

[43] Xin Yan, Chihiro Kito, Shohei Miyoshi, Meisong Liao, Takenobu Suzuki, and Yasutake Ohishi. Raman transient response and enhanced soliton self-frequency shift in ZBLAN fiber. *J. Opt. Soc. Am. B*, 29(2):238–243, Feb 2012.